Highly efficient removal of Pb^{2+} from aqueous solution using polyaniline-cobalt composite nanorods: Kinetics, isotherm and mechanistic investigation

Madhumita Bhaumik [a], Arjun Maity [b c], H.G. Brink [a]

[a]Department of Chemical Engineering, Faculty of Engineering, Built Environment and Information Technology, University of Pretoria, Pretoria, South Africa
[b]DST/CSIR, Centre for Nanostructure and Advanced Materials (CeNAM), Council for Scientific and Industrial Research (CSIR), Pretoria, 0001, South Africa
[c]Institute for Nanotechnology and Water Sustainability, University of South Africa, Florida Park, Roodepoort, 1709, South Africa

* Corresponding author. Email: bhaumikmadhu@gmail.com

Highlights

- Novel composite nanorods of polyaniline and cobalt (PANI-Co CNRs) were synthesized.

F0B7 - PANI-Co CNRs displayed outstanding removal capacity for Pb^{2+} from aqueous solution.

F0B7 - Adsorption isotherms revealed an exothermic reaction at an optimal pH of 5.0.

F0B7 - Rapid sorption kinetics of Pb^{2+} removal followed pseudo-first-order kinetic model.

F0B7 - Adsorption/precipitation and successive reduction to Pb^{0} were the prime mechanism.

Abstract

Nanosized cobalt (Co) particles exhibit unique chemical, magnetic, electronic, and catalytic properties. Like nanoscale metallic iron, nanostructured Co and its composite nanostructures also show significant potential for the removal of toxic metal cations from water and wastewater. To explore this potential, composite nanorods (CNRs) of nanosized Co immobilized polyaniline (PANI) nanorods (NRs) matrix (PANI-Co CNRs) were synthesized and effectively applied for the treatment of lead ions (Pb^{2+}), serving as a model for heavy metal pollutants in water bodies. Physico-chemical characterization of PANI-Co CNRs revealed that weak ferromagnetic Co nanoparticles (NPs) were effectively deposited onto the surface of the PANI NRs. The enhanced surface properties and superior reactivity of PANI-Co CNRs resulted in greater Pb^{2+} removal efficiency compared to their individual components. The adsorption kinetics were notably rapid, with the time required to reach equilibrium varying between 60 and 150 min for initial concentrations ranging from 50 to 150 mg/L, all at a pH of 5.0. The isotherm data revealed an impressive Pb^{2+} adsorption capacity of 1130 mg/g at 25 °C, as determined using the non-linear Langmuir model. Exothermic and spontaneous Pb^{2+} removal process was deduced from the thermodynamic investigations. Among co-contaminating metal ions, only Cu^{2+} ions significantly affected the Pb^{2+} removal performance of the PANI-Co CNRs, implying its possible applications in decontaminating industrial effluent laden with various metal ions. Mechanistic investigation revealed that the treatment process primarily

involves the adsorption and precipitation of Pb^{2+} onto the surface of PANI-Co CNRs, followed by its subsequent reduction to form metallic Pb (Pb^0).

Graphical abstract

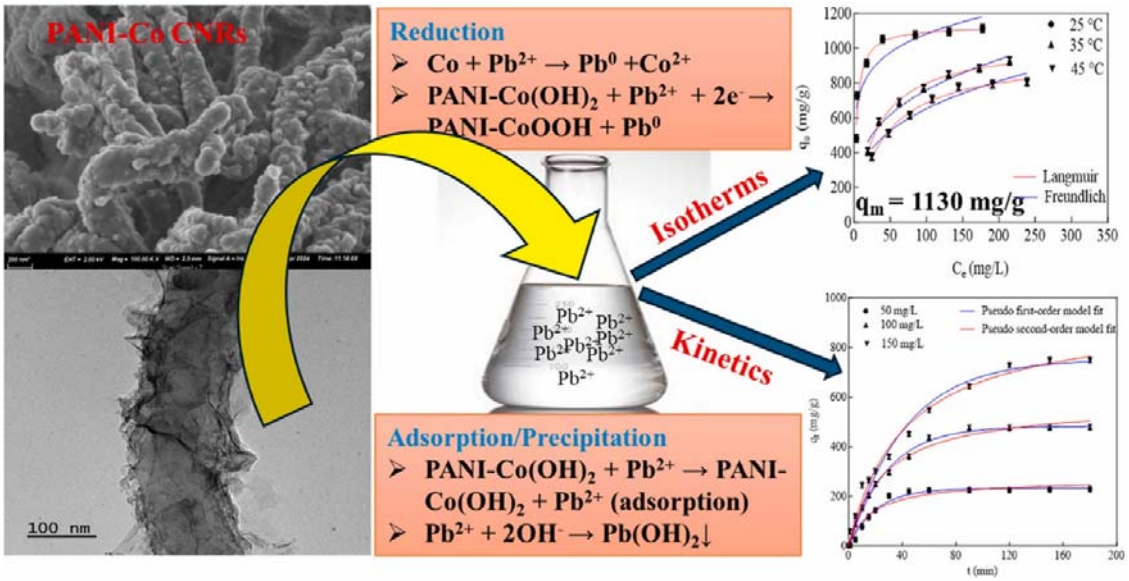

Keywords: Polyaniline nanorods; Nanosized Co; $Pb^{2+;}$ Adsorption; Kinetics; Isotherm

1. Introduction

Water pollution by both inorganic and organic contaminants is a significant global environmental challenge. Among these, heavy metal pollutants are particularly concerning due to their high toxicity and potential harm to human health and ecosystems. Lead, in its ionic form (Pb^{2+}), is especially problematic, as it is a major hazardous metal with severe environmental impacts. Industries such as paint and pigment manufacturing, mining, electroplating, and battery production frequently discharge wastewater with elevated Pb^{2+} levels, leading to contamination of aquatic environments. Even trace amounts of Pb^{2+} in drinking water can cause serious health issues, including nausea, kidney failure, cancer, and neurological disorders (Reddy and Lee, 2013). Due to the serious health risks associated with lead exposure, the U.S. Environmental Protection Agency (EPA) has set the maximum allowable limit for Pb^{2+} discharge in drinking water at 15 µg/L (Chowdhury et al., 2022), whereas the World Health Organization (WHO) has established a guideline of 10 µg/L as the maximum tolerable levels of Pb^{2+} in drinking water (Guidelines for drink, 2011).

Consequently, various treatment techniques involving ion exchange, chemical precipitation, reverse osmosis, bioremediation, and adsorption have conventionally been employed towards the removal of Pb^{2+} from industrial wastewater (Fu and Wang, 2011; Renu et al., 2017). Innate advantages such as easy operational procedure, higher pollutant removal efficiency, accessibility of various adsorbents, and low cost have made adsorption one of the most attractive technologies for the decontamination of Pb^{2+} loaded wastewaters (Yu et al., 2017; Li et al., 2019). Choosing an effective adsorbent with high affinity for contaminant ions and a rapid sorption rate is crucial for the successful operation of a sorption system. In this

regard, nanomaterials, with their enhanced surface properties and numerous exposed reaction sites, are excellent candidates for superior adsorption. Consequently, the use of nano-adsorbents has increased significantly in recent years. However, in practical applications, especially in continuous flow systems like mixed vessels and fixed-bed columns, these nanomaterials often face significant challenges, including agglomeration, difficulty in separation from solutions, and excessive pressure drop (Savage and Diallo, 2005; Hua et al., 2012; Hotze et al., 2010). Agglomeration of nanoparticles can be reduced to a certain extent by supporting or immobilising in high surface area porous matrix such as on nanocarbons or functional polymers matrix. Meanwhile, nanoparticles with magnetic properties employed to synthesize magnetic nanocomposite adsorbents facilitate their simple separation after pollutant removal from treated water using an electromagnet. Therefore, various magnetic nanoparticles and their composites have been applied for the treatment of Pb^{2+} in water/wastewater (Irawan et al., 2019; Ge et al., 2012; Nata et al., 2010; Şahin et al., 2023; Chen et al., 2016). Nonetheless, most of these magnetic nano adsorbents have minimal or moderate capacities in removing Pb^{2+} ions from water (Kim et al., 2013a; Zhang et al., 2013a; Ge et al., 2018; Bhaumik et al., 2021). Therefore, it remains crucial to develop innovative magnetic nanocomposite adsorbents that possess both high sorption capacity and rapid removal rates for Pb^{2+}.

Conducting polymers, particularly polyaniline (PANI) in its nanostructured form, have garnered significant attention from researchers due to their simple and controllable synthesis in bulk quantities for a variety of advanced technological applications (Long et al., 2011; Singh and Shukla, 2020; Tanguy et al., 2018; Banerjee et al., 2019). Additionally, high surface area, proper functionality, good environmental stability has made nanostructured PANI an excellent matrix for supporting magnetic nanoparticles (Bhaumik et al., 2014). Meanwhile, nanocomposites composed of nanostructured PANI, and magnetic nanoparticles offer advantages such as good suspension ability, high affinity for removing targeted contaminants, and rapid separation capability.

In this study, a magnetic composite nanostructure composed of nanorod-shaped PANI and nanosized Co, designated as PANI-Co composite nanorods (CNRs), was fabricated using a facile technique. Due to the presence of negatively charged SO_3^- groups of 2-NSA doped PANI polymer, it attracts electrostatically positively charged Co^{2+} ions which upon reduction produced strongly attached Co NPs onto the polymer surface. Both SO_3^- groups and formed Co NPS are expected to have strong affinity towards the removal of Pb^{2+} ions. To prove this CNRs were effectively used for the first time to remove Pb^{2+} from water samples. The synthesis of PANI-Co magnetic CNRs involved the initial chemical synthesis of PANI nanorods, followed by the reductive deposition of Co NPs onto the pre-synthesized PANI matrix. Various physico-chemical techniques were employed to characterize the PANI-Co CNRs. Experiments for Pb^{2+} removal were conducted in batch sorption mode, with variations in several operational parameters. Finally, the mechanism of Pb^{2+} removal was explored in detail.

2. Materials and methods

2.1. Materials

The monomer aniline (≥99.5%) used for synthesis of PANI homopolymer was obtained from Sigma Aldrich, USA, and stored at 0–5 °C before use. Other chemicals used in the study, also purchased from Sigma Aldrich, USA, include the dopant 2-naphthalene sulfonic acid (technical grade, 70%), the oxidant ammonium persulfate (ACS reagent, ≥98%), the metal precursor cobalt chloride hexahydrate, the reducing agent hydrazine hydrate (50–60%), ethylene glycol (EG), lead(II) nitrate (ACS reagent, ≥99.0%), cadmium(II) chloride (anhydrous, ≥99.0%), zinc(II) nitrate hexahydrate (≥98%), copper(II) sulfate pentahydrate, sodium hydroxide, potassium hydroxide, calcium chloride, magnesium chloride and nitric acid. These chemicals were used as received.

2.2. Procedure of PANI nanorods synthesis

PANI nanorods (NRs) doped with 2-naphthalene sulfonic acid were prepared using a simple chemical polymerization technique. In a typical polymerization process within deionized (DI) water (80 mL), aniline monomer (0.2 mL) and 2-naphthalene sulfonic acid (0.416 g) were mixed by magnetic stirring at 0–5 °C for 30 min. Afterwards, an aqueous oxidant solution (0.456 g ammonium persulfate in 10 mL DI water) was added to the mixture and stirring continued for an additional minute. Subsequently, the polymerization mixture was kept under static conditions at 0–5 °C for 24 h. Upon completion of the reaction, the PANI polymer was separated from the reaction mixture by vacuum filtration. Finally, the polymer was obtained by washing with DI water and methanol, followed by drying in a vacuum oven at 60 °C for 24 h.

2.3. PANI-Co composite nanorods synthesis

The PANI-Co CNRs was synthesized by reductive immobilization of nanosized metallic Co onto the previously synthesized PANI NRs surface/matrix. The immobilization of nanosized Co particles onto the PANI NRs surface was performed as follows:

Initially, 0.403 g of $CoCl_2 \cdot 6H_2O$ was dissolved in 20 mL of ethylene glycol (EG). The PANI NRs (0.2 g) were then well-dispersed in this solution through ultrasonic agitation. For the reductive formation of metallic Co NPs, hydrazine hydrate (10 mL) and sodium hydroxide solution (1 M, 4 mL) were added to the PANI-Co^{2+} suspension. This reduction reaction led to the formation of Co NPs on the PANI NRs surface/matrix. The entire reduction reaction was carried out at a temperature of 70 °C. The resulting PANI-Co CNRs (containing approximately 30 wt% Co) were filtered, washed with DI water and ethanol, and then vacuum dried for 24 h at 60 °C. Bare Co NPs were also prepared using a similar reduction protocol for comparison.

2.4. Characterization instruments

Morphological characterization along with size estimation of the prepared PANI NRs and PANI-Co CNRs were performed with a field emission-scanning electron microscope (FE-SEM, Zeiss-ULTRA plus, Germany) and a high-resolution-transmission electron microscope (HR-

TEM), JEOL JEM-2100, Japan. The surface properties of the PANI NRs and PANI-Co CNRs were achieved by a Micromeritics (UK) ASAP 2420 N_2 adsorption-desorption technique. Various functional groups of the prepared nanomaterials were identified using Fourier transform infrared (FTIR) spectra, acquired by an attenuated total reflection (ATR) Spectrum 100 FTIR spectrometer, PerkinElmer, USA. A powder X-ray diffractometer (Panalytical X'Pert PRO) was employed for obtaining crystalline information of the PANI-Co CNRs before as well as after Pb^{+2} adsorption. The elements present onto the surface of PANI-Co CNRs and the oxidation state of the formed Co NPs were explored from the X-ray photoelectron spectra (XPS) obtained by a XPS spectrometer, ESCALAB 250Xi, Thermo Scientific (USA) equipped with an Al monochromatic X-ray source. The Vibrating Sample Magnetometer (VSM) measurement option of a Physical Property Measurements System (PPMS Evercool-II, Quantum Design, USA) was used to acquire magnetic property curve of the PANI-Co CNRs at room temperature.

2.5. Pb^{2+} removal experiments

For the preparation of 1000 mg/L stock solution of Pb^{2+} an appropriate amount of $Pb(NO_3)_2$ was dissolved in 1000 mL DI water. All solutions for experiments with desired concentrations of Pb^{2+} were obtained by diluting the stock solution. Batch equilibrium experiments for Pb^{2+} adsorption was performed by agitating the water samples in a temperature-controlled incubator shaker at 200 rpm for 24 h. Assessment of the Pb^{2+} removal efficiencies of various adsorbents were conducted by varying the doses of Co NPs, PANI NRs and PANI-Co CNRs within 100 mg/L Pb^{2+} solution (50 mL) at its original pH (5.2) in a100 mL glass container. The effect of solution pH within the range of 2.0–6.0 on Pb^{2+} removal efficiency of the PANI-Co CNs was examined through mixing 0.2 g/L of adsorbent in 100 mg/L Pb^{2+} solution at 25 °C for 24 h. The initial pH of the samples was adjusted with 0.1 M HNO_3 and/or 0.1 M NaOH solutions. The efficiency (removal %) of Pb^{2+} adsorption was determined by utilizing Eq. (1):

$$\text{Removal } \% = \left(\frac{C_0 - C_e}{C_0} \right) \times 100 \quad (1)$$

where C_0 and C_e represent initial and the equilibrium concentration of Pb^{2+} in mg/L unit.

Adsorption kinetics was conducted by contacting 0.05 g of PANI-Co CNRs with 250 mL of Pb^{2+} solution at a pH of 5.0 and agitated at 200 rpm speed. The initial concentration of the solution was varied in the 50–150 mg/L range, whereas the temperature of the solution was fixed at 25 °C. On pre-determined time periods a specific amount of reaction solution was withdrawn and filtered by a nylon syringe filter with 0.22 µm pore size. After filtration the residual Pb^{2+} concentration in the solution was analysed with PerkinElmer's AAnalyst-400 AA, atomic absorptions spectrometer. The time-dependent Pb^{2+} removal capacity of PANI-Co CNRs was calculated by employing Eq. (2):

$$q_t = \left(\frac{C_0 - C_t}{m} \right) V \quad (2)$$

where, q_e represents adsorption capacity (mg/g) of the adsorbent at a specified period t, C_t in mg/L denotes bulk-phase adsorbate concentration at any time t and m (g)is the adsorbent mass.

To evaluate the effect of temperature on Pb^{2+} uptake of PANI-Co CNRs, the equilibrium isotherm experiments were performed at three different temperatures (25, 35 and 45 °C). For a particular temperature, the initial concentrations of Pb^{2+} were varied from 100 mg/L to 400 mg/L, while the dose and the pH of the solutions were kept constant at 0.2 g/L and 5.0, respectively. The equilibrium Pb^{2+} adsorption capacity of PANI-Co CNRs was calculated by employing Eq. (3):

$$q_e = \left(\frac{C_0 - C_e}{m}\right) V \tag{3}$$

where, q_e stands for equilibrium adsorption capacity in mg/g; V signifies volume of the sample in L; and m is the mass (g) of the adsorbent.

Effect of other co-contaminating heavy metal ions on the removal of Pb^{2+} using PANI-Co CNRs was examined with a binary ions' adsorption methodology. Cadmium (Cd^{2+}), Copper (Cu^{2+}), zinc (Zn^{2+}) are the respective studied co-existing ions along with Pb^{2+}. Accordingly, 50 mL aqueous solution containing Pb^{2+}/Cu^{2+}, Pb^{2+}/Zn^{2+} and Pb^{2+}/Cd^{2+} were mixed with PANI-Co CNRs (0.01 g) at 25 °C for 24 h. In the binary ion's solution, each of the co-existing heavy metal ions concentration was varied from 50 mg/L −150 mg/L, whereas the concentration of Pb^{2+} was kept constant at 100 mg/L. On reaching adsorption equilibrium the experimental solutions were analysed for the determination of remaining Pb^{2+} concentration. Additionally, the effect of common metal ions such as Na^{+}, K^{+}, Ca^{2+} and Mg^{2+} were also tested in binary sorption mode to evaluate their effects on Pb^{2+} ion removal performance of PANI-Co CNRs. In the binary sorption experiments initial concentrations of Na^{+}, K^{+}, $Ca^{2+}$and Mg^{2+} were varied from 50 to 100 mg/L whereas Pb^{2+} concentration was maintained at 100 mg/L. After equilibration time the samples were analysed for Pb^{2+} concentrations.

The recyclability/reusability of PANI-Co CNRs was tested by repetitive Pb^{2+} adsorption and desorption experiments for three consecutive cycles. Initially, 50 mL of 100 mg/L Pb^{2+} solution was prepared. Then 0.01 g of adsorbent was contacted with the Pb^{2+} solution. The mixture was shaken at 25 °C for 2 h. The desorption process was in 50 mL deionized water for 24 h. The filtrate from each cycle was measured for residual Pb^{2+} concentration.

3. Results and discussion

3.1. Characterization

A representative image of the synthesized pristine PANI polymer, as obtained by FE-SEM, is shown in Fig. 1a. The image reveals the formation of rod-shaped PANI with diameters ranging from 151 to 254 nm. Following the immobilization/dispersion of nanosized Co, the diameter of the PANI NRs increased from 184 nm to 294 nm, as demonstrated in Fig. 1b of the PANI-Co CNRs. It is noteworthy from Fig. 1b that the surface of the PANI-Co CNRs appears rougher compared to the bare PANI NRs. Typical images of the pure PANI NRs along with PANI-Co CNRs as acquired by HR-TEM are shown in Fig. 2a–d. From Fig. 2b and c, it can be observed that predominantly Co nanocrystals are unevenly distributed on the amorphous PANI NRs (Fig. 2a) surface. The lattice fringes with 0.21 nm inter planer or d spacing, as observed in the high-resolution image (Fig. 2d) of PANI-Co CNRs, corresponded to the face centred cubic (111)

crystal planes of metallic Co, demonstrating the highly crystalline structure of the formed Co NPs. Elemental mapping, as acquired from energy dispersive X-ray spectroscopy (EDS) confirmed the presence of carbon (C), nitrogen (N), and sulphur (S) associated primarily with PANI NRs, and cobalt (Co) corresponding to the metallic Co deposits (Fig. S1, supplementary figure).

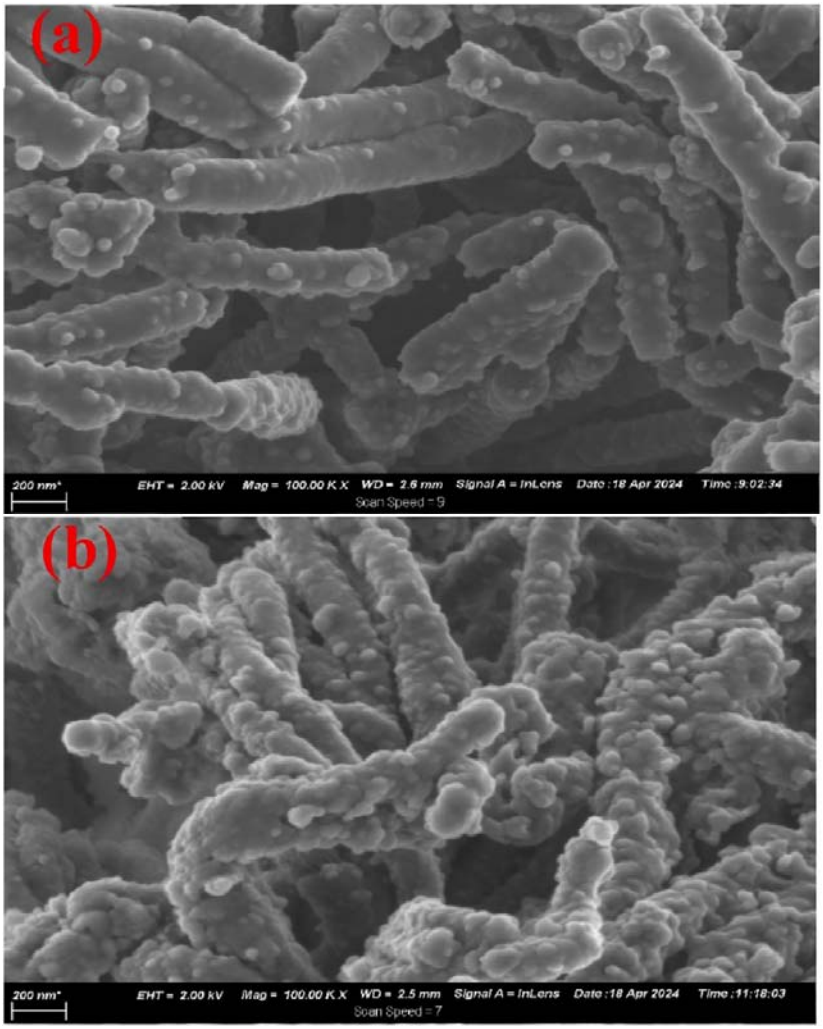

Fig. 1. FE-SEM images of (a) PANI NRs and (b) PANI-Co CNRs.

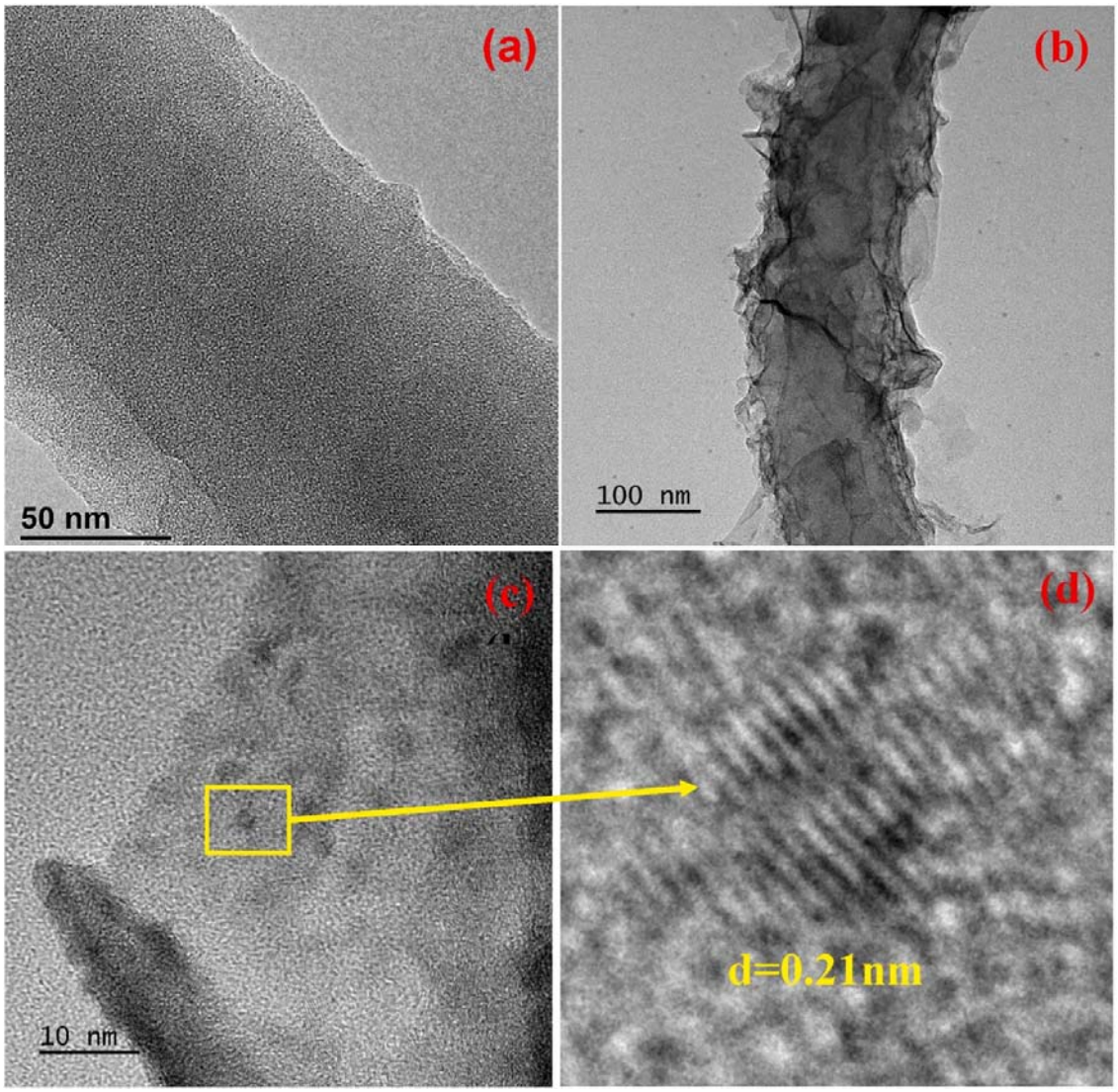

Fig. 2. HR-TEM image of (a) PANI NRs; (b) and (c) PANI-Co CNRs at two different magnifications; (d) Crystal lattice fringe of Co NPs within PANI-Co CNRs.

The specific surface areas of the PANI-Co CNRs and pristine PANI NRs as determined by the BET method of N_2 adsorption-desorption isotherms (Fig. S2, supplementary figure) were measured as 26.7 and 19.09 m^2/g, respectively. The considerable enhancement in the specific surface area of the PANI-Co CNRs compared to the PANI NRs indicates a greater availability of interfacial area for solid-liquid interactions. This increased surface area likely contributes to the improved performance in contaminant removal. Furthermore, the estimated respective average pore diameters of the PANI-Co CNRs and PANI NRs are 17.5 and 13.9 nm. The acquired averaged size of the pores are in the 2–50 nm range, characterizing their meso-porosity. Large surface area and high porosity facilitate rapid diffusion of absorbate ions and therefore favourable for effective adsorption of pollutants.

In Fig. S3(a), supplementary figure, (ATR-FTIR spectrum) the characteristic bands appearing at 1568, and 1485 cm^{-1} are representative of the stretching vibration of the quinoid (Q) and

benzenoid (B) rings within the PANI polymer. The bands detected at 1297 and 1240 cm^{-1} can be attributed to vibrational stretching of the C and N bonds of Q-B-Q as well as B components whereas 1129 and 805 cm^{-1} bands correspond to the stretching and bending vibrations of respective B–NH^{+} = Q, and C–H units of the aromatic rings within the PANI backbone (Huang and Wan, 1999). The existing bands at 1023 and 670 cm^{-1} confirm the absorption/doping of sulfonic acid (-SO_3H) groups from 2-naphthalene sulfonic acid to PANI structure during the polymerization reaction (Bhaumik et al., 2018). Meanwhile, it can also be identified from FTIR spectrum of PANI-Co (Fig. 3a) that all the FTIR peaks representing the 2-naphthalene sulfonic acid doped PANI polymer were moved towards higher wave number when Co NPs were deposited on its surface. This might be because of the weak van der Waals force acting between PANI matrix and the as grown Co NPs.

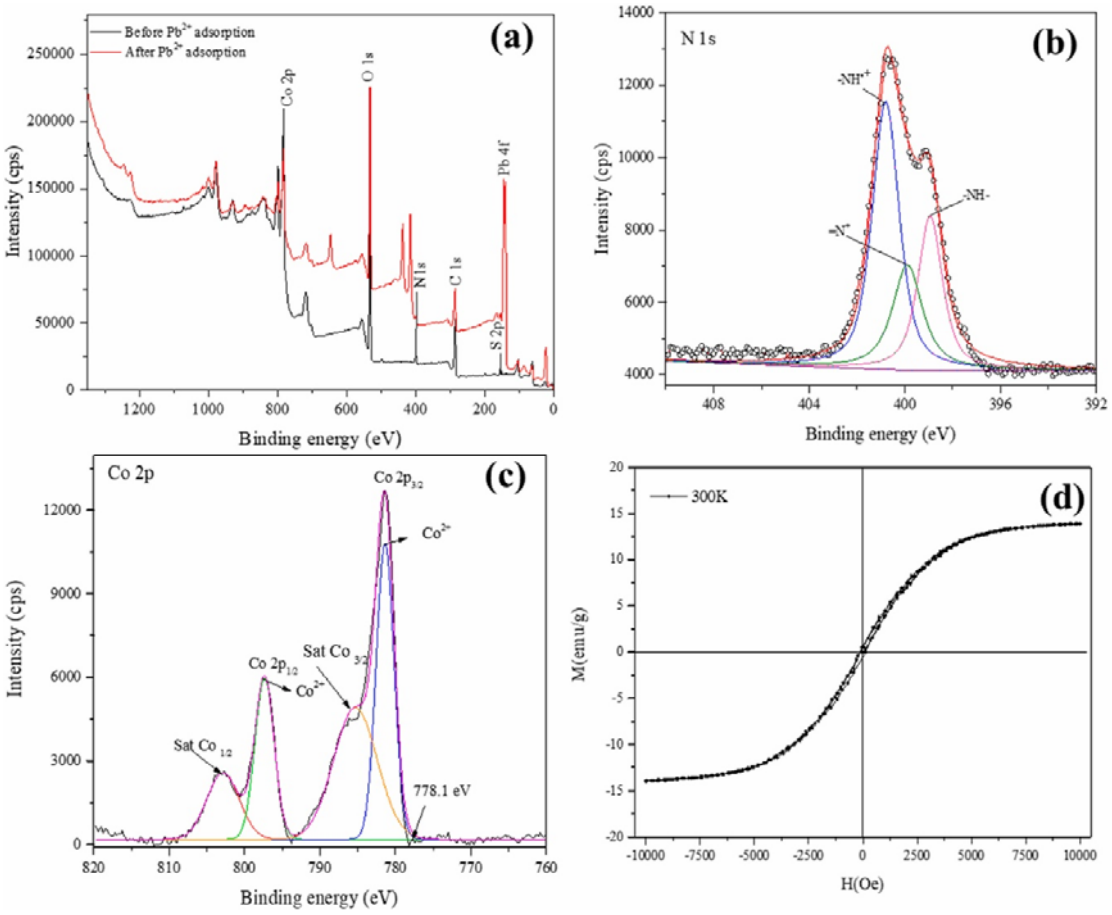

Fig. 3. (a) XPS survey spectra of PANI-Co CNRs before and after removal of Pb^{2+}, (b) N1s core level spectrum of PANI-Co CNRs, (c) Co 2p spectrum of PANI-Co CNRs before Pb^{2+} removal and (d) M – H curve of PANI-Co CNRs at 300K.

The XRD curve of the PANI-Co CNRs is depicted in Fig. S3(b), supplementary figure. The sharp peak obtained at 2θ value of 44.2° along with minor peaks at around 51.4° and 75.7° appeared due to the diffraction from (111), (200) and (220) crystalline planes of metallic Co (JCPDS cards No. 15–0806). These XRD peaks indicate successful immobilization/supporting of metallic Co NPs onto the PANI NRs surface. Additionally, a broad peak ranging from 20.01° to 27.3° revealing amorphous feature of the synthesized PANI NRs (Zhang et al., 2005).

The exploration of elemental species on the surface of the PANI-Co CNRs and the oxidation state of the as-grown Co NPs were conducted through X-ray photoelectron spectroscopy (XPS) analysis. The XPS survey scan of the PANI-Co CNRs is shown in Fig. 3a. In the survey spectrum, peaks corresponding to C 1s, N 1s, S 2p and O 1s binding energies were observed, indicating the presence of the PANI polymer component. The Co 2p peak, on the other hand, originated from the deposited Co NPs. These findings demonstrate that the elements present on the surface of the composite nanostructures originate from both the PANI NRs and Co NPs components. The high-resolution N 1s binding energy peak, as shown in Fig. 3b, is deconvoluted into three distinct peaks. The respective peaks with binding energies centred at 398.9, 399.8, and 400.8 eV are attributed to imine nitrogen (-N =) units, benzenoid amine (–NH–) units, and cationic nitrogen atoms ($–NH^{•+}$) in the PANI polymer (Wei et al., 1999). These results suggest successful doping of 2-naphthalene sulfonic acid during PANI formation. The core-level spectrum of Co 2p, as shown in Fig. 3c, features respective doublets (Co $2p_{3}/_{2}$ and Co $2p_{1}/_{2}$) arising from multi-electron excitations. Specifically, the primary Co $2p_{3}/_{2}$ peak at 781.2 eV and the Co $2p_{1}/_{2}$ peak at 797.3 eV, along with their satellite peaks at 785.3 eV (sat Co $2p_{3}/_{2}$) and 802.8 eV (sat Co $2p_{1}/_{2}$), suggest the presence of Co^{2+} species in the form of $Co(OH)_{2}$ on the PANI-Co CNRs surface (Kim and Choo, 2007). Additionally, the binding energy peak around 778.1 eV, corresponding to Co $2p_{3}/_{2}$ and attributable to metallic Co, was barely noticeable due to the high surface sensitivity of the XPS technique, which is limited to a depth of less than 10 nm (Zhao et al., 2013). These observations further suggest that the metallic Co NPs immobilized onto the surface of PANI were coated with a thin $Co(OH)_2$ layer.

The potential for magnetic separation of the PANI-Co CNRs from the bulk solution after contaminant removal was assessed by measuring their magnetic properties at room temperature. Fig. 3d shows the room temperature (300 K) magnetization (M) versus magnetic field strength (H) curve for the PANI-Co CNRs. The presence of a thin hysteresis loop with a saturation magnetization (M_s) value of 13.9 emu/g and a magnetic coercivity (H_c) of 139.6 Oe indicates weakly ferromagnetic behaviour of the prepared PANI-Co CNRs, demonstrating their suitability for easy magnetic separation (Fig. S4, supplementary figure) from water after pollutant removal.

3.2. Assessment of Pb^{2+} removal performance of Co NPs, PANI NRs and PANI-Co CNRs

PANI-Co CNRs, pristine PANI NRs, and bare Co NPs were examined for the comparison of their Pb^{2+} adsorption efficiencies. Fig. S5(a), supplementary figure, describes the Pb^{2+} removal performance (removal %) at different doses of PANI-Co CNRs, Co NPs and pristine PANI NRs. It is noteworthy from Fig. S5(a), supplementary figure, that at 0.01 g/50 mL dose 99.49 % of Pb^{2+} removal efficiency was attained by the PANI-Co CNRs, whereas only 36.76 % and 67.28 % removal performance were achieved by PANI NRs and Co NPs, respectively. These results suggests that Pb^{2+} adsorption from aqueous solution using PANI-Co CNRs was more effective than that of bare Co NPs and PANI NRs counterparts. The enhanced Pb^{2+} removal performance of PANI-Co CNRs is attributed to its larger external surface area, which provides more available area for solid-liquid interactions compared to its individual components. Additionally, the use of PANI NRs as a support matrix prevented the aggregation of magnetic Co NPs during composite formation, thereby improving the reactivity of the material toward Pb^{2+} removal using their synergistic effect (Bhaumik et al., 2021). The observed increase in Pb^{2+} removal performance with higher amounts (masses) of each adsorbent is associated with

the greater accessibility of active sites at higher doses. Meanwhile, even though the tolerance limit of cobalt is 0.05 mg/L for the potable water (Chi et al., 2019), preliminary leaching test in the pH range 5–6 of the PANI-Co CNRs showed that concentration of leached Co^{2+} in the treated water was 0.018 mg/L which is well below the maximum permissible limit. Therefore, the PANI-Co CNRs can be considered as an environmentally friendly adsorbent for the removal of Pb^{2+}.

3.3. Impact of initial solution pH

The initial pH of the metal ion solution is a crucial parameter that significantly influences removal performance. This is because it affects the nature of the charged species formed on the surface of the adsorbent, thereby governing the type of interactions between the sorbate ions in the aqueous solution and the adsorbent's surface species. The Pb^{2+} removal efficiency (removal %) of the PANI-Co CNRs at various pH values of the solution is illustrated in Fig. S5(b). The performance of PANI-Co CNRs for Pb^{2+} removal was significantly lower at pH values of 2–3, while a substantial improvement in removal efficiency was observed within the pH range of 4–6. The Pb^{2+} removal efficiency remained relatively stable across pH values from 4 to 6, varying from 99.43 % at pH 4–99.95 % at pH 6, as shown in Fig. S5(b). These results indicate that strongly acidic conditions are not favourable for Pb^{2+} removal using PANI-Co CNRs. This disparity in Pb^{2+} removal performance at different initial pH of the solution can be justified by considering point-of-zero charge (PZC) value of the PANI-Co CNRs, which is at pH 4.89 as portrayed in Fig. S5(c), supplementary figure. The surface of the PANI-Co CNRs adsorbent acquires to be positively charged (protonated) below the pH of PZC (pH_{PZC}) and beyond it the surface remains deprotonated or negatively charged. Therefore, in the lower pH range ($pH < pH_{PZC} = 4.89$) electrostatic repulsion of positively charged surface sites along with competitive interaction between H^+ and Pb^{2+} ions decrease the Pb^{2+} removal efficiency. Additionally, under acidic conditions, the supported Co NPs are more likely to corrode, reducing their reactivity and, consequently, their performance in Pb^{2+} removal (Zhang et al., 2010). In contrast, increasing the solution pH from 5 to 6 reduced the effect of competitive adsorption and enhanced the adsorption efficiency of PANI-Co CNRs for Pb^{2+}. Moreover, under weakly acidic conditions, the oxidation of metallic Co NPs in the presence of dissolved oxygen and water generates a significant number of OH^- ions. This increases the reaction solution pH, as shown in Fig. S5(b), and promotes the precipitation of Pb^{2+} as $Pb(OH)_2$, thereby contributing to improved Pb^{2+} removal performance.

3.4. Adsorption kinetics

The kinetic performance of the PANI-Co CNRs towards Pb^{2+} adsorption at three distinct initial concentrations is displayed in Fig. 4. Rapid Pb^{2+} removal using PANI-Co CNRs is observed with enhanced adsorption capacity corresponding to the increased initial concentrations. Meanwhile, the time required to reach equilibrium adsorption varied from 30 to 120 min as the concentration of Pb^{2+} ions increased from 50 mg/L to 150 mg/L. Rapid Pb^{2+} ions removal is achieved through substantially exposed reactive surface sites of the PANI-Co CNRs possessing considerable higher surface area. Additionally, from Fig. 4, it can be noticed that the initial rate of Pb^{2+} removal from solution was considerably faster compared to the later stage.

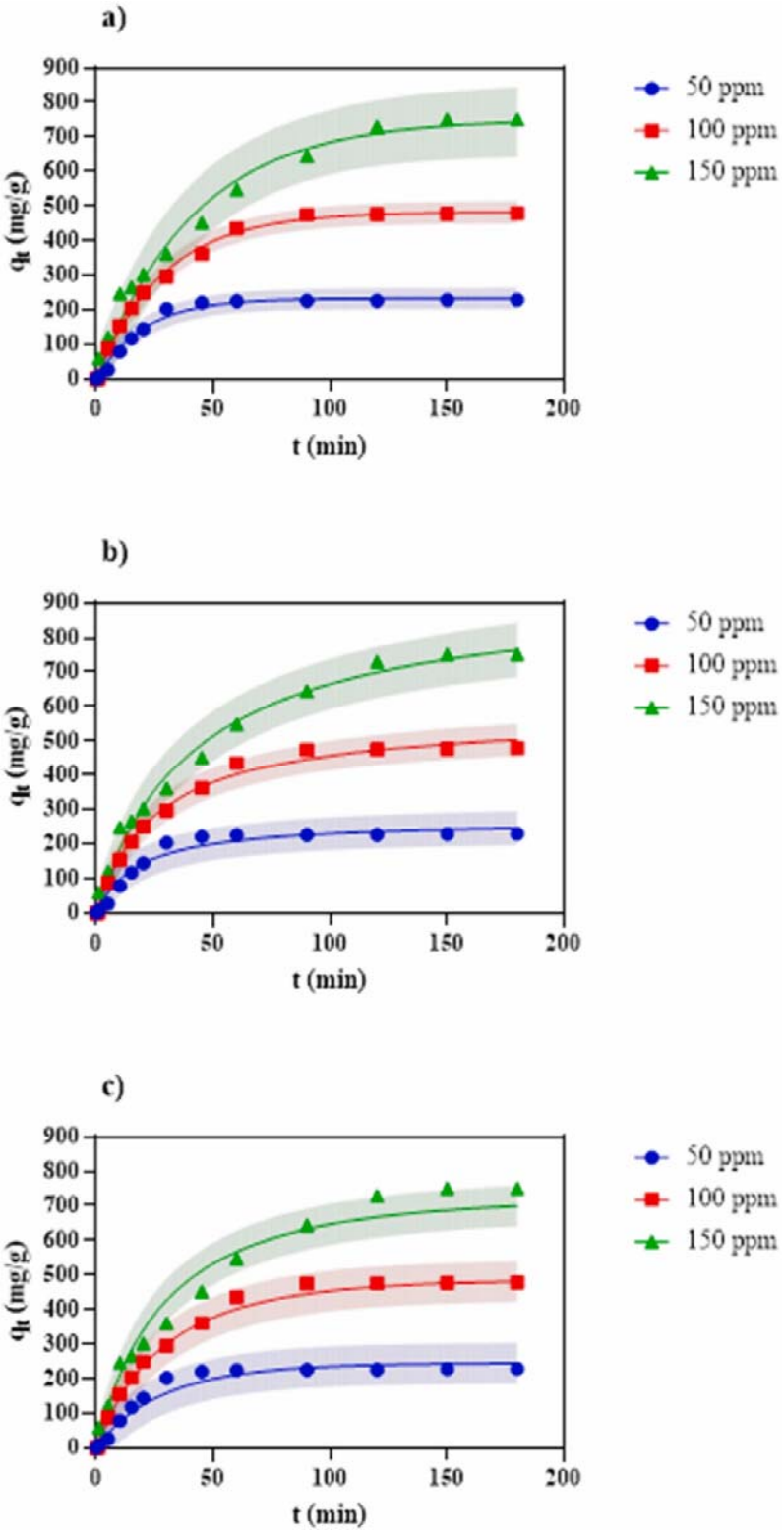

Fig. 4. The effect of contact time on adsorption of Pb^{2+} by PANI-Co CNRs and the fitting of kinetic data with non-linear a) pseudo-first-order, b) pseudo-second-order, and c) Langmuir kinetic models (dose: 0.2 g/L, pH: 5.0). The shaded area represents the 95% prediction interval which represents the region with a 95% probability of future observations.

The assessment of the mechanism involved in the kinetics of Pb^{2+} removal was carried out by analysing the experimental kinetic data using three widely applied theoretical models: the pseudo-first-order, pseudo-second-order, and Langmuir kinetic models (Muedi et al., 2021; Lohrentz et al., 2023). The non-linear forms of these models can be expressed by the following equations:

$$\frac{dq_t}{dt} = k_1 \left(q_e - q_t\right) \tag{4}$$

$$\frac{dq_t}{dt} = k_2 (q_e - q_t)^2 \tag{5}$$

$$\frac{dq_t}{dt} = k_{ad} \left(C_o - q_t \frac{W}{V}\right) \left(1 - \frac{q_t}{q_m}\right) - \frac{k_{ad}}{b} \frac{q_t}{q_m} \tag{6}$$

where k_1, k_2 and k_{ad} are the respective rate constants associated with pseudo-first-order, pseudo-second-order, and Langmuir reaction kinetics. *W* represents the mass of adsorbent loaded and *V* the volume of solution, while q_m and *b* were obtained from the equilibrium values fitted for the Langmuir isotherm as reported in Table S1, supplementary table. The experimental kinetic data fitted with Eqs. (4), (5), (6) are shown in Fig. 4. The values of correlation coefficients (R^2) obtained from non-linear regression analysis, used to assess the best fitting kinetic model, are presented in Table S1, supplementary table. The higher values of the R^2 (≈0.984–0.995) for the pseudo-first-order kinetic model, in comparison with the pseudo-second-order model (R^2 ≈ 0.958–0.991), imply its superiority in describing empirical kinetic data. Well conformity of the experimental kinetic data with the pseudo-first-order kinetic model suggests that physical adsorption is the rate-determining step for the current sorption system (Irani et al., 2013). A similar kinetic mechanism (pseudo-first-order) was observed for Pb^{2+} removal using supported nanoscale zero-valent iron by Ponder et al., 2000) (Ponder et al., 2000). Meanwhile, the associated values of the kinetic rate constants (Table S1) for Pb^{2+} removal by PANI-Co CNRs decreased with increasing initial concentration.

Additionally, despite the relatively lower R^2 value of 0.983 for the Langmuir kinetic model compared to the pseudo-first-order model, the Langmuir model holds significant value as a mechanistic model. One of its key advantages is its ability to scale the reaction kinetics independently of the initial concentration of the adsorbate or the reactor configuration. This is extremely powerful because it supports the scalability of the model, allowing it to predict the kinetics for different initial concentrations using a single parameter (k_{ad}) (Muedi et al., 2021; Lohrentz et al., 2023; Scott Fogler, 2013). This attribute is crucial for practical applications, as it provides a more flexible and generalizable framework for scaling up the process from lab-scale experiments to industrial-scale operations. The fact that all three initial concentrations could be predicted by a single parameter (k_{ad}) underscores the robustness and practical applicability of the Langmuir kinetic model in real-world scenarios.

3.5. Adsorption isotherm

The isotherm data obtained under adsorption equilibrium conditions are crucial for determining the maximum adsorption capacity of a specific adsorbent. These data are also

vital for designing an effective adsorption process, as it provides insights into how the adsorbent interacts with the adsorbate at various concentrations, enabling optimization of the adsorption conditions for maximum efficiency. The isotherm data for equilibrium Pb^{2+} adsorption by the PANI-Co CNRs at three experimental temperatures (25, 35, and 45 °C) are shown in Fig. 5. It is noteworthy that the Pb^{2+} adsorption capacity of the PANI-Co CNRs increases with decreasing temperature, indicating the exothermic nature of the adsorption process. The non-linear and linear forms of the Langmuir and Freundlich isotherm models can be presented by Eqs. (7)–(10), respectively:

$$q_e = \frac{q_m b C_e}{1+bC_e} \tag{7}$$

$$\frac{C_e}{q_e} = \frac{1}{q_m b} + \frac{C_e}{q_m} \tag{8}$$

$$q_e = K_F C_e^{1/n} \tag{9}$$

$$\ln\ q_e = \ln\ k_F + \frac{1}{n}\ln\ C_e \tag{10}$$

where q_m (mg/g), b (L/mg), k_F ((mg/g)(L/mg)$^{1/n}$), and n denote respective maximum adsorption capacity, sorption free energy, Freundlich isotherm constant associated with adsorption capacity and adsorption intensity. The fitted curves of the experimental isotherm data with non-linear and linear Langmuir and Freundlich isotherm models are exhibited through Fig. 5 and S6. The respective isotherm parameters as obtained using linear and non-linear regression method of the experimental data for three distinct temperatures are represented in Table 1. Higher values of R^2 obtained for both the linear and non-linear Langmuir models compared to the Freundlich model suggest that the Langmuir model better describes the experimental isotherm data. This result implies that Pb^{2+} removal primarily occurs through monolayer formation on the homogeneous surface sites of the adsorbent. Meanwhile, the q_m values of Pb^{2+} sorption onto the PANI-Co CNRs surface declines from 1130 (or 1111.1) to 960.1 (or 909.09) mg/g for temperature rise from 25 to 45 °C. This finding further signifies that the interaction between sorption sites of the PANI-Co CNRs sorbent and Pb^{2+} would be enhanced on lowering the reaction temperature. Similarly, the b values lessen from 0.2819(0.272) to 0.0251 (0.0272) for the rise in temperature from 25 to 45 °C, is indicative of the significantly improved affinity towards Pb^{2+} sorption of the PANI-Co CNRs at lower temperature. The q_m values of various magnetic nanocomposites along with PANI-Co CNRs for Pb^{2+} removal, recently reported (Jabeen et al., 2013; Kim et al., 2013b; Peng et al., 2014; Liu et al., 2015; Du et al., 2019; Nicola et al., 2020; Qu et al., 2021) are presented in Table S2, supplementary table. The q_m value of PANI-Co CNRs is substantially greater than most of the reported magnetic adsorbents. Excellent sorption capacity, simple and economical synthesis method suggest potential applicability of PANI-Co CNRs towards removal of Pb^{2+} from environmental/industrial wastewater stream.

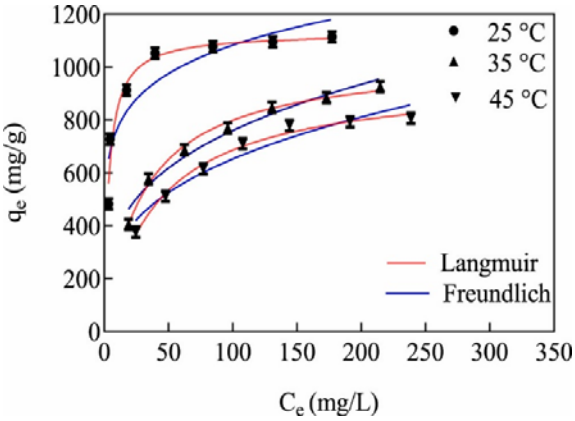

Fig. 5. Equilibrium isotherms of Pb^{2+} removal onto PANI-Co CNRs and non-linear fitting of isotherm data with Langmuir and Freundlich models. (Initial conc.: 50–400 mg/L, dose: 0.2 g/L and pH: 5.0).

Table 1. Langmuir and Freundlich isotherm model parameters for Pb^{2+} adsorption by the PANI-Co CNRs.

Isotherm Mode	**Temperature**		
	25 °C	**35 °C**	**45 °C**
Langmuir			
Linea			
q_m	1111.1	1000	909.09
B	0.272	0.0335	0,0272
R^2	0.999	0.998	0.997
Non-linear			
Best-fit values			
q_m	1130	1036	960.1
B	0.2819	0.0337	0.0251
Std. Error			
q_m	31.37	18.12	22.76
B	0.0446	0.0022	0.0021
95% Confidence Intervals			
q_m	1015–1212	990.5–1085	904.7–1022
B	0.1909–0.4341	0.0284–0.041	0.0202–0.0312
Goodness of Fit			
Degrees of Freedom	5	5	5
R^2	0.9555	0.9934	0.9899
Absolute Sum of Squares	15086	1380	1618
Sy.x	54.93	16.61	17.99
Number of points Analysed	7	7	7
Freundlich			
Linear			
k_F	489.06	170.54	132.19
n	5.675	3.081	2891
R^2	0.807	0.962	0.958
Non-Linear			
k_F	540.6	192.3	154.1
n	6.629	3.351	3.191

Std. Error			
k_F	75.01	24.18	28.20
N	1.460	0.2966	0.3816
95% Confidence Intervals			
k_F	369.0–743.5	138.5–261.4	95.52–239.5
N	4.188–13.97	2.726–4.284	2.437–4.50
Goodness of Fit			
Degrees of Freedom	5	5	5
R^2	0.8343	0.9695	0.9455
Absolute Sum of Squares	56200	6339	8736
Sy.x	106.0	35.61	41.80
Number of points Analysed	7	7	7

Units: q_m: mg/g, b: L/mg, K_F: ((mg/g)(mg/L)$^{-1/n}$).

3.6. Evaluation of thermodynamic parameters

Three commonly explored thermodynamic parameters such as change in Gibbs free energy (ΔG^0), change of entropy (ΔS^0) and enthalpy change (ΔH^0) for adsorption of Pb^{2+} by PANI-Co CNRs were obtained by utilizing the following expressions:

$$\Delta G^0 = -RT \ln K_c \tag{11}$$

$$\ln K_c = \frac{\Delta S^0}{R} - \frac{\Delta H^0}{RT} \tag{12}$$

where R (8.314 J mol^{-1} K^{-1}) denotes universal gas constant, T is the temperature in K and stands for equilibrium constant. The plot of lnKc versus 1/T used to calculate ΔG^0, ΔS^0 and ΔH^0 values is shown in Fig. S7, supplementary figure. Table S3, supplementary table summarizes the obtained values of three thermodynamic parameters. An exothermic process of Pb^{2+} adsorption is confirmed from the negative value of ΔH^0. This further signifies more Pb^{2+} adsorption by PANI-Co CNRs on lowering the temperature than that by elevating the temperature. In the meantime, negative values of ΔG^0 infers spontaneity of Pb^{2+} sorption onto the PANI-Co CNRs surface. Furthermore, negative value of ΔS^0 suggests declined randomness at the solid-liquid interface in the present removal process.

3.7. Effect of co-existing metal ions

Various industrial processes, such as battery manufacturing, electroplating, automotive, steel production, and aeronautics, release effluents containing substantial amounts of Pb^{2+} along with other heavy metal ions, including Cd^{2+}, Cu^{2+}, and Zn^{2+}. Consequently, the influence of these co-existing metal ions on Pb^{2+} sorption by PANI-Co CNRs were studied in a binary-ions sorption mode. Pb^{2+} adsorption performance of PANI-Co CNRs from the binary sorption systems of Cd^{2+}/Pb^{2+}, Cu^{2+}/Pb^{2+} and Zn^{2+}/Pb^{2+} at three different initial concentrations are depicted in Fig. S8(a), supplementary figure. It can be seen in Fig. S8(a), supplementary figure, that without other co-existing heavy metal ions ~99.9% of Pb^{2+} removal was achieved from 100 mg/L aqueous solution utilizing 0.2 g/L of PANI-Co CNRs. On the other hand, decreased removal % of Pb^{2+} is observed in presence of Cu^{2+} ions with various initial Cu^{2+} concentrations for the binary ion sorption mode. Specifically, 68.3%, 50.35% and 43.87% of Pb^{2+} removal was

obtained in presence of 50, 100 and 150 mg/L of Cu^{2+}. Meanwhile minor change in Pb^{2+} removal efficiencies are observed in presence of Cd^{2+} and Zn^{2+}at their three different initial concentrations. These results suggest competitive adsorption performance for various metal ions using PANI-Co CNRs adsorbent that pursues the sequence of Pb^{2+}>Cu^{2+}>Cd^{2+}> Zn^{2+}. The bivalent Cu^{2+} ions could effectively competitively bind to the adsorption sites based on the Jahn-Teller effect, which leads to the reduction in Pb^{2+} removal performance of PANI-Co CNRs (Zhao et al., 2019). However, no significant change in Pb^{2+} removal efficiencies were observed in presence of Na^{+}, K^{+}, Ca^{2+} and Mg^{2+} ions as presented in Fig. S7(b), supplementary figure. This might be due to the less affinity of the respective ions towards the sorption sites of PANI-Co CNRs compared to the Pb^{2+} ions. Therefore, marginal reduction in Pb^{2+} adsorption efficiency for the co-existing metal ions confirms the feasibility of PANI-Co CNRs in treating industrial effluent.

3.8. Recyclability of PANI-Co CNRs

Recyclability/Reusability of the spent adsorbent is an important factor in order to evaluate the cost effectiveness of the material for industrial applications. The Pb^{2+} removal efficiency of the PANI-Co CNRs undergoing three adsorption-desorption cycles are presented in Fig. S9, supplementary figure. It is noteworthy that PANI-Co CNRs retains its original 99.99% removal efficiency for two consecutive adsorption cycles, whereas in the third adsorption cycle Pb^{2+} removal efficiency was diminished to 71.17%. Therefore, the PANI-Co CNRs could be reused for two successive adsorption-desorption cycles without loss of its original removal performance. The decline in removal efficiency in the third cycle might be result of exhaustion of Co nanoparticles by repeated chemical reactions and small amount of leaching as well as incomplete resolution of adsorbed Pb^{2+} ions from the surface of the adsorbent (Yang et al., 2018).

3.9. Mechanistic exploration of Pb^{2+} removal by PANI-Co CNRs

The removal mechanism of Pb^{2+} from aqueous solution using PANI-Co CNRs was explored by employing the XRD and XPS results. The XRD curve (Fig. 6a) of PANI-Co CNRs after the removal of Pb^{2+}, displays the change in typical diffraction peaks relative to the detected peaks (Fig. S2(b)) before adsorption process. The peaks observed at 24.61°, 27.03° and 32.86° are the characteristic peaks of $Pb(OH)_2$, while the peak at 34.11° is attributable to the diffraction peak of $PbO{\cdot}xH_2O$ (JCPDS: 00-001-0270). The peaks, observed at 35.94°, 55.5° and 62.1° are typical of metallic Pb or Pb^0 (Ponder et al., 2000). Meanwhile, peaks at 2θ values of 58.2°, 60,4° and 62.1° suggesting the presence of $PbCO_3$ (JCPDS: 00-003-0358). $PbCO_3$ might be produced due to the interaction between Pb^{2+} and dissolve carbon dioxide (Liu et al., 2019) in water. The appearance of the various Pb species in the XRD pattern of PANI-Co CNRs after adsorption indicates involvement of various mechanisms in the removal process. In aqueous solution at higher pH (∼5.0) value metallic Co of PANI-Co CNRs oxidized to Co^{2+} species which governs adsorptive removal of Pb^{2+} and its subsequent conversion into $Pb(OH)_2$ and $PbO{\cdot}xH_2O$ (Ponder et al., 2000). Furthermore, since the standard reduction potential of Pb^{2+}/Pb^0 (−0.1263 V) is less negative than that of Co^{2+}/Co^0 (−0.277 V), some of the Pb^{2+} in the solution reduced to Pb^0 by the electrochemical process (Zhang et al., 2011). Therefore, the electrochemically produced Pb^0 were effectively deposited onto the PANI-Co CNRs surface as revealed by the XRD analysis. The XPS survey scan of the PANI-Co CNRs after contact with aqueous Pb^{2+} is

presented in Fig. 4a. Occurrence of Pb 4f binding energy peak in Fig. 3a suggests that Pb species were immobilized onto the surface of PANI-Co CNRs. Core level spectrum of Pb 4f, depicted in Fig. 6b consists of peaks associated with respective Pb $4f_{5/2}$ and Pb $4f_{7/2}$ orbitals. The photoelectron peak centred at about 138.2 eV, attributable to Pb $4f_{7/2}$ is in conformity with reported binding energy peak for Pb^{2+} sequestration using nano scale zero valent iron (Zhang et al., 2013b). In contrast, the peak about 143 eV is in the vicinity of the stated 143.1 eV binding energy peak of Pb $4f_{5/2}$ (Liu et al., 2019). These two peaks confirm the presence of lead oxides/hydroxide onto the surface of PANI-Co, which is in accordance with the XRD result (Liu et al., 2015). Irrespective of the occurrence of elemental lead (Pb^0) in the XRD curve, non-appearance of it from the Pb 4f core level spectrum is attributable to the facts of air oxidation and surface passivation of the generated Pb^0, leads to the presence of Pb^{2+} oxidized species only. The high-resolution Co 2p peak of PANI-Co CNRs after removal of Pb^{2+} is presented in Fig. 6c. The decomposed Co $2p_{3/2}$ peaks stipulate that the binding energy peak located at 782.3 eV is marginally altered towards higher energy value in comparison with

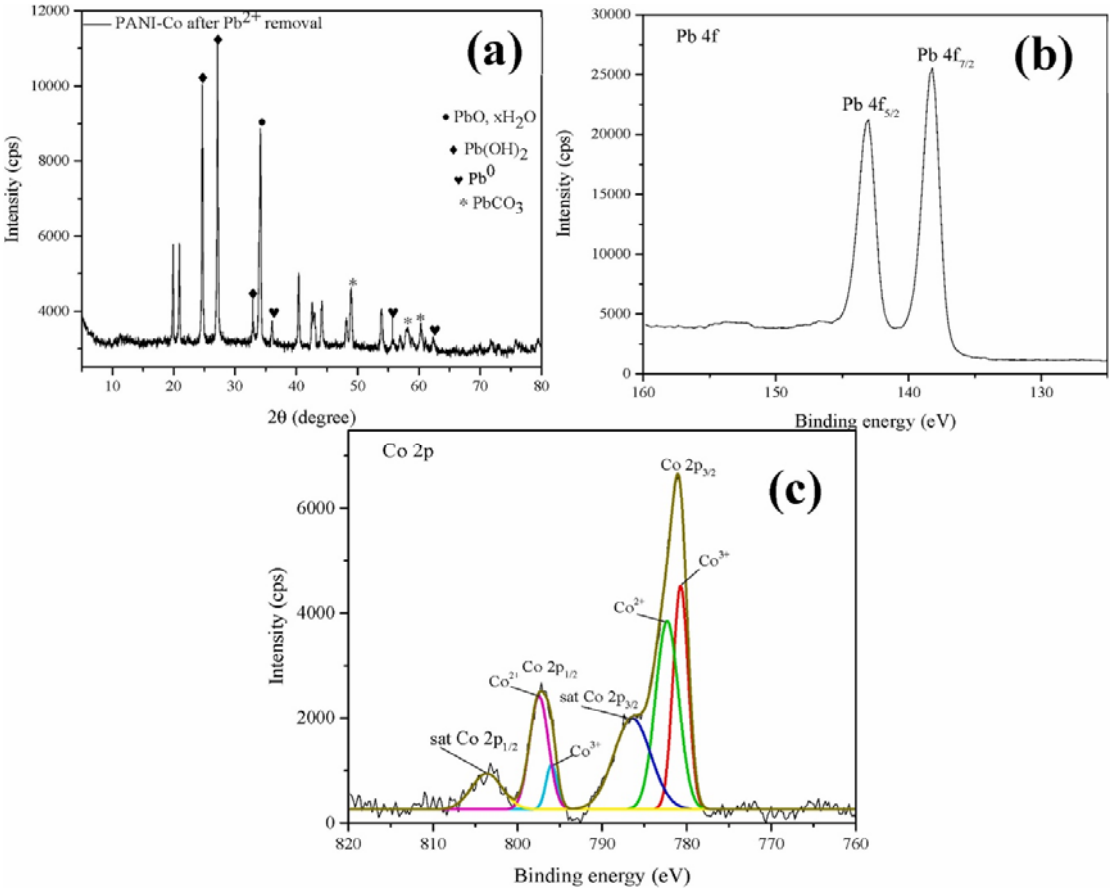

Fig. 6. (a) XRD pattern of PANI-Co CNRs after removal of Pb^{2+} and high resolution XPS spectra of Pb 4f (b) and Co 2p (c) after removal of Pb^{2+} by PANI-Co CNRs**.**

Co $2p_{3/2}$ peak at 781.4 eV preceding to treatment with Pb^{2+} aqueous solution. Furthermore, appearance of 780.7 eV and 795.9 eV binding energy peaks, consistent with the +3-oxidation state of Co in the form of CoOOH (Menezes et al., 2015), recommends engagement of Co^{2+} species on the reduction of Pb^{2+} to form Pb^0 species. On the basis of the XRD and XPS analyses

results the plausible mechanism of Pb^{2+} removal by PANI-Co CNRs could be described by multiple steps. Firstly, direct precipitation of $Pb(OH)_2$, formed via the reaction of aqueous Pb^{2+} and OH^- ions generated on reduction of H_2O by the immobilized Co NPs as presented by the following expressions:

$$Co + 2H_2O \rightarrow Co^{2+} + H_2 \uparrow + 2OH^- \quad (13)$$

$$Co + 2H_2O + 1/2\ O_2 \rightarrow Co^{2+} + 4OH^- \quad (14)$$

$$Pb^{2+} + 2OH^- \rightarrow Pb(OH)_2 \downarrow \quad (15)$$

Secondly, adsorption of Pb^{2+} on the surface sites of the adsorbent, represented as follows:

$$Co^{2+} + 2OH^- \rightarrow Co(OH)_2 \quad (16)$$

$$PANI\text{-}Co(OH)_2 + Pb^{2+} \rightarrow PANI\text{-}Co(OH)_2 + Pb^{2+}\ (adsorption) \quad (17)$$

Thirdly, negatively charged SO_3^- groups of 2-NSA doped PANI polymer attracts electrostatically positively charged Pb^{2+} ions and thus contributing a reactive support matrix towards the removal of Pb^{2+} ions. Finally, some of the formed Pb^{2+} species were transformed to Pb^0 through direct electrochemical reduction process and by in situ generated Co^{2+}, as illustrated below:

$$Co + Pb^{2+} \rightarrow Pb^0 + Co^{2+} \quad (18)$$

$$PANI\text{-}Co(OH)_2 + Pb^{2+} + 2e^- \rightarrow PANI\text{-}CoOOH + Pb^0 \quad (19)$$

Therefore, the simultaneous presence of both Pb^o and Pb^{2+} species on the PANI-Co CNRs surface after the treatment experiment indicates that the mechanisms involved in Pb^{2+} removal from water include precipitation, adsorption, and subsequent reduction.

4. Conclusions

In this work, composite nanorods (CNRs) composed of PANI and Co were efficiently prepared through a straightforward reductive immobilization process, where metallic Co NPs were supported on a PANI polymer matrix. The synthesized weakly ferromagnetic PANI-Co CNRs were effectively used for the highly efficient removal of Pb^{2+} from aqueous solutions. The PANI-Co CNRs demonstrated superior efficiency, achieving a 99.6% removal for Pb^{2+}, compared to 77.5% for unsupported Co NPs and 51.2% for pristine PANI NRs. The adsorption process was rapid, with kinetic data best described by the pseudo-first-order model, and the rate constant increased as the initial concentration of Pb^{2+} decreased. Despite the relatively lower R^2 value of 0.983 compared to the pseudo-first-order model, the Langmuir kinetic model's ability to predict kinetic behaviour across different initial concentrations using a single parameter highlights its scalability and practical applicability. The process was exothermic, with a maximum adsorption capacity of 1130 mg/g for Pb^{2+} at 25 °C, as determined by the non-linear fitting of isotherm data using the Langmuir model. The presence of co-existing Cu^{2+} significantly affected the Pb^{2+} removal performance due to the high affinity

of PANI-Co CNRs for Cu^{2+}, suggesting the feasibility of PANI-Co CNRs for treating industrial effluents containing various metal cations. Detailed XRD and XPS analyses revealed that the removal mechanisms involve surface adsorption/precipitation of Pb^{2+} ions by the reactive PANI-Co CNRs and the reductive formation of Pb^{o} by the Co NPs.

CRediT authorship contribution statement

Madhumita Bhaumik: Writing – original draft, Visualization, Validation, Methodology, Investigation, Formal analysis, Data curation, Conceptualization. **Arjun Maity:** Writing – review & editing, Visualization, Validation, Project administration, Methodology, Investigation. **H.G. Brink:** Writing – review & editing, Validation, Project administration, Funding acquisition.

Declaration of competing interest

The authors declare that they have no known competing financial interests or personal relationships that could have appeared to influence the work reported in this paper.

Acknowledgements

Financial support from the University of Pretoria (UP) and National Research Foundation (NRF), South Africa are thankfully acknowledged by MB, AM and HGB. The Department of Physics, University of South Africa is also acknowledged for providing their Magnetic characterization facility. The work was further supported by the Austrian Federal Ministry of Education, Science and Research (BMBWF) through Austria's Agency for Education and Internationalization (OeAD) [Grant numbers: Africa UNINET P056, P058 and APPEAR Project 341].

Data availability

No data was used for the research described in the article.

References

Banerjee, J., Dutta, K., Kader, M.A., Nayak, S.K., 2019. An overview on the recent developments in polyaniline-based supercapacitors. Polym. Adv. Technol. 30, 1902–1921.

Bhaumik, M., Choi, H.J., McCrindle, R.I., Maity, A., 2014. Composite nanofibers prepared from metallic iron nanoparticles and polyaniline: high performance for water treatment applications. J. Colloid Interface Sci. 425, 75–82.

Bhaumik, M., Gupta, V.K., Maity, A., 2018. Synergetic enhancement of Cr(VI) removal from aqueous solutions using polyaniline@$Ni(OH)_2$ nanocomposites adsorbent. J. Environ. Chem. Eng. 6, 2514–2527.

Bhaumik, M., Maity, A., Brink, H.G., 2021. Zero valent nickel nanoparticles decorated polyaniline nanotubes for the efficient removal of Pb(II) from aqueous solution: synthesis, characterization and mechanism investigation. Chem. Eng. J. 417, 127910.

Chen, D., Awut, T., Liu, B., Ma, Y., Wang, T., Nurulla, I., 2016. Functionalized magnetic Fe_3O_4 nanoparticles for removal of heavy metal ions from aqueous solutions. E-Polymers 16, 313–322.

Chi, L., Wang, Z., Sun, Y., Lu, S., Yao, Y., 2019. Removal of cobalt ions from wastewater by Friedel's salt. Mater. Res. Express 6, 015508.

Chowdhury, I.R., Chowdhury, S., Mazumder, M.A.J., Al-Ahmed, A., 2022. Removal of lead ions (Pb^{2+}) from water and wastewater: a review on the low-cost adsorbents. Appl. Water Sci. 12, 185.

Du, Y., Dai, M., Cao, J., Peng, C., 2019. Fabrication of a low-cost adsorbent supported zero-valent iron by using red mud for removing Pb(II) and Cr(VI) from aqueous solutions. RSC Adv. 9, 3348.

Fu, F., Wang, Q., 2011. Removal of heavy metals from waste waters: a review. J. Environ. Manag. 92, 407–418.

Ge, F., Li, M.M., Ye, H., Zhao, B.X., 2012. Effective removal of heavy metal ions Cd^{2+}, Zn^{2+}, Pb^{2+}, Cu^{2+} from aqueous solution by polymer-modified magnetic nanoparticles. J. Hazard Mater. 211–212, 366–372.

Ge, L., Wang, W., Peng, Z., Tan, F., Wang, X., Chen, J., Qiao, X., 2018. Facile fabrication of Fe@ MgO magnetic nanocomposites for efficient removal of heavy metal ion and dye from water. Powder Technol. 326, 393–401.

Guidelines for drink-water quality, WHO Chron. 4 (2011) 383.

Hotze, E.M., Phenrat, T., Lowry, G.V., 2010. Nanoparticle aggregation: challenges to understanding transport and reactivity in the environment. J. Environ. Qual. 39, 1909–1924.

Hua, M., Zhang, S., Pan, B., Zhang, W., Lv, L., Zhang, Q., 2012. Heavy metal removal from water/wastewater by nanosized metal oxides: a review. J. Hazard Mater. 211–212, 317–331.

Huang, J., Wan, M., 1999. In situ doping polymerization of polyaniline microtubules in the presence of β-naphthalene sulfonic acid. J. Polym. Sci.: Polym. Chem. 37, 151–157.

Irani, A.M., Ismaeili, J., Piri, H., Parnian, M.J., 2013. Electrospun nanofiber membrane of PEO/chitosan for the adsorption of nickel, cadmium, lead and copper ions from aqueous solution. Chem. Eng. J. 220, 237–243.

Irawan, C., Nata, I.F., Lee, C.K., 2019. Removal of Pb(II) and As(V) using magnetic nanoparticles coated montmorillonite via one-pot solvothermal reaction as adsorbent. J. Environ. Chem. Eng. 7, 103000.

Jabeen, H., Kemp, K.C., Chandra, V., 2013. Synthesis of nano zerovalent iron nanoparticles-graphene composite for the treatment of lead contaminated water. J. Environ. Manag. 130 (2013), 429–435.

Kim, M.H., Choo, K.H., 2007. Low-temperature continuous wet oxidation of trichloroethylene over CoOx/TiO2 catalysts. Catal. Commun. 8, 462–466.

Kim, S.A., Kamala-Kannan, S., Lee, K.J., Park, Y.J., Shea, P.J., Lee, W.H., Kim, H.M., Oh, B.T., 2013a. Removal of Pb(II) from aqueous solution by a zeolite–nanoscale zero-valent iron composite. Chem. Eng. J. 217, 54–60.

Kim, S.A., Kamala-Kannan, S., Lee, K.J., Park, Y.J., Shea, P.J., Lee, W.H., Kim, H.M., Oh, B.T., 2013b. Removal of Pb(II) from aqueous solution by a zeolite–nanoscale zero-valent iron composite. Chem. Eng. J. 217, 54–60.

Li, L., Liu, X., Xu, J., Kan, C., 2019. Microfluidic preparation of thiol-containing monodisperse polymer microspheres and their adsorption of Pb^{2+} in water. Chem. Eng. J. 375, 122012.

Liu, M., Wang, Y., Chen, L., Zhang, Y., Lin, Z., 2015. $Mg(OH)_2$ supported nanoscale zero valent iron enhancing the removal of Pb(II) from aqueous solution. Appl. Mater. Interfaces 7, 7961–7969.

Liu, X., Lai, D., Wang, Y., 2019. Performance of Pb(II) removal by an activated carbon supported nanoscale zero-valent iron composite at ultralow iron content. J. Hazard Mater. 361, 37–48.

Lohrentz, L., Bhaumik, M., Brink, H.G., 2023. High-capacity adsorption of hexavalent chromium by a polyaniline-Ni(0) nanocomposite adsorbent: expanding the Langmuir-Hinshelwood kinetic model. J. Mol. Liq. 389, 122931.

Long, Y.Z., Li, M.M., Gu, C., Wan, M., Duvail, J.L., Liu, Z., Fan, Z., 2011. Recent advances in synthesis, physical properties and applications of conducting polymer nanotubes and nanofibers. Prog. Poly. Sci. 36, 1415–1442.

Menezes, P.W., Indra, A., Gonzalez-Flores, D., Sahraie, N.R., Zaharieva, I., Schwarze, M., Strasser, P., Dau, H., Driess, M., 2015. High-performance oxygen redox catalysis with multifunctional cobalt oxide nanochains: morphology-dependent activity. ACS Catal. 5, 2017–2027.

Muedi, K.L.L., Brink, H.G., Masindi, V., Maree, J.P.P., 2021. Effective removal of arsenate from wastewater using aluminium enriched ferric oxide-hydroxide recovered from authentic acid mine drainage. J. Hazard Mater. 414, 125491.

Nata, I.F., Salim, G.W., Lee, C.K., 2010. Facile preparation of magnetic carbonaceous nanoparticles for Pb^{2+} ions removal. J. Hazard Mater. 183, 853–858.

Nicola, R., Costisor, O., Ciopec, M., Negrea, A., Lazău, R., Ianăsi, C., Piciorus, E.M., Len, A., Almásy, L., Szerb, E.I., Putz, A.M., 2020. Silica-coated magnetic nanocomposites for Pb^{2+} removal from aqueous solution. Appl. Sci. 10, 2726.

Peng, X., Xu, F., Zhang, W., Wang, J., Zeng, C., Niu, M., Chmielewská, E., 2014. Magnetic Fe_3O_4 @ silica–xanthan gum composites for aqueous removal and recovery of Pb^{2+}. Colloids Surf. A Physicochem. Eng. Asp. 443, 27–36.

Ponder, S.M., Darab, J.G., Mallouk, T.E., 2000. Remediation of Cr(VI) and Pb(II) aqueous solutions using supported, nanoscale zerovalent iron. Environ. Sci. Technol. 34, 2564–2569.

Qu, J., Liu, Y., Cheng, L., Jiang, Z., Zhang, G., Deng, F., Wang, L., Han, W., Zhang, Y., 2021. Green synthesis of hydrophilic activated carbon supported sulfide nZVI for enhanced Pb(II) scavenging from water: characterization, kinetics, isotherms and mechanisms. J. Hazard Mater. 403, 123607.

Reddy, D.H.K., Lee, S.M., 2013. Three-dimensional porous spinel ferrite as an adsorbent for Pb(II) removal from aqueous solutions. Ind. Eng. Chem. Res. 52, 15789–15800.

Renu, M. Agarwal, Singh, K., 2017. Heavy metal removal from wastewater using various adsorbents: a review. J. Water Reuse Desalin. 7, 387–419.

Şahin, M., Atasoy, M., Arslan, Y., Yildiz, D., 2023. Removal of Ni(II), Cu(II), Pb(II), and Cd(II) from aqueous phases by silver nanoparticles and magnetic nanoparticles/nanocomposites. ACS Omega 8, 34834–34843.

Savage, N., Diallo, M.S., 2005. Nanomaterials and water purification: opportunities and challenges. J. Nanopart. Res. 7, 331–342.

Scott Fogler, H., 2013. Elements of Chemical Reaction Engineering. Fourth.; Pearson Education Limited, London. ISBN 0130473944.

Singh, P., Shukla, S.K., 2020. Advances in polyaniline-based nanocomposites. J. Mater. Sci. 55, 1331–1365.

Tanguy, N.R., Thompson, M., Yan, N., 2018. A review on advances in application of polyaniline for ammonia detection. Sensors Actuators B Chem. 257, 1044–1064.

Wei, X.L., Fahlman, M., Epstein, A.J., 1999. XPS study of highly sulfonated polyaniline. Macromolecules 32, 3114–3117.

Yang, F., Zhang, S., Sun, Y., Cheng, K., Li, J., Tsang, D.C.W., 2018. Fabrication and characterization of hydrophilic corn stalk biochar-supported nanoscale zero-valent iron composites for efficient metal removal. Bioresour. Technol. 265, 490–497.

Yu, C., Shao, Z., Hou, H., 2017. A functionalized metal–organic framework decorated with O groups showing excellent performance for lead(II) removal from aqueous solution. Chem. Sci. 8, 7611–7619.

Zhang, Z., Wei, Z., Zhang, L., Wan, M., 2005. Polyaniline nanotubes and their dendrites doped with different naphthalene sulfonic acids. Acta Mater. 53, 1373–1379.

Zhang, X., Lin, S., Lu, X.Q., Chen, Z., 2010. Removal of Pb(II) from water using synthesized kaolin supported nanoscale zero-valent iron. Chem. Eng. J. 163, 243–248.

Zhang, X., Lin, S., Chen, Z., Megharaj, M., Naidu, R., 2011. Kaolinite-supported nanoscale zero-valent iron for removal of Pb2+ from aqueous solution: reactivity, characterization and mechanism. Water Res. 45, 3481–3488.

Zhang, Y., Su, Y., Zhou, X., Dai, C., Keller, A.A., 2013a. A new insight on the core-shell structure of zerovalent iron nanoparticles and its application for Pb(II) sequestration. J. Hazard Mater. 263, 685–693.

Zhang, W., Shi, X., Zhang, Y., Gu, W., Li, B., Xian, Y., 2013b. Synthesis of water-soluble magnetic graphene nanocomposite for recyclable removal of heavy metal ions. J. Mater. Chem. A. 1, 1745–1754.

Zhao, L., Liao, K., Pynenburg, M., Wong, L., Heinig, N., Thomas, J.P., Leung, K.T., 2013. Electro-oxidation of ascorbic acid by cobalt Core Shell nanoparticles on a H-terminated Si(100) and by nanostructured cobalt-coated Si nanowire electrodes. ACS Appl. Mater. Interfaces 5, 2410–2416.

Zhao, X., Wang, Y., Li, Y., Xue, W., Li, J., Wu, H., Zhang, Y., Li, B., Liu, W., Gao, Z., Huang, H., 2019. Synergy effect of pore structure and amount of carboxyl site for effective removal of Pb2+ in Metal Organic frameworks. J. Chem. Eng. Data 64, 2728–2735.